

# Molecular, spectroscopic and thermal studies on catechol, 4,5-dibromocatechol, resorcinol, hydroquinone and 4-4'-dihydroxybiphenyl derivatives armed with benzothiazole moieties

Arwa Alshargabi<sup>a</sup>, Guan-Yeow Yeap<sup>a,\*</sup>, Wan Ahmad Kamil Mahmood<sup>a</sup>, Rakesh Samikannu<sup>b</sup>

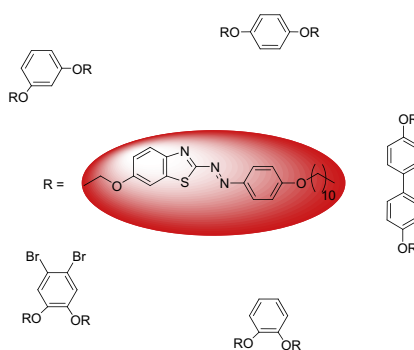
<sup>a</sup>Liquid Crystal Research Laboratory, School of Chemical Sciences, Universiti Sains Malaysia, 11800 Minden, Penang, Malaysia

<sup>b</sup>Department of Chemistry, Anna University, Chennai, Tamil Nadu 600 025, India

## HIGHLIGHTS

- ▶ Benzothiazole based liquid crystals synthesized.
- ▶ The structural evaluation by <sup>1</sup>H–<sup>1</sup>H COSY, <sup>1</sup>H–<sup>13</sup>C HMBC and <sup>1</sup>H–<sup>13</sup>C HMQC.
- ▶ All compound exhibited nematic phase.

## GRAPHICAL ABSTRACT



## ARTICLE INFO

### Article history:

Received 14 October 2012

Received in revised form 14 January 2013

Accepted 17 January 2013

Available online 13 February 2013

### Keywords:

Catechol

Resorcinol

Hydroquinone

Liquid crystal dimers

2D NMR spectroscopy

Thermal behavior

## ABSTRACT

A new series of catechol, 4,5-dibromocatechol, resorcinol, hydroquinone and 4-4'-dihydroxybiphenyl derivatives possessing two benzothiazole moieties at respective positions of 1,2, 1,3, 1,4 and/or 4,4' has successfully been synthesized. The molecular structures were fully elucidated by spectroscopic techniques (<sup>1</sup>H NMR, <sup>13</sup>C NMR and two dimensional COSY, HMBC, HMQC, DEPT-135 and DEPT-90). The connectivity study between the cause of using different core systems in the target compounds and the anisotropic behavior as inferred from phase transition temperature and relevant morphology studies has led to some unique features arising from this series. Compounds with *ortho* substituent exhibit enantiotropic N and SmA phases. The analogues containing resorcinol and 4,4'-disubstituentbiphenyl show enantiotropic nematic behavior while the hydroquinone derivative induces the formation of monotropic nematogen. An extensive study to further substantiate the relationship between the stability of the nematic phase and associated transition temperatures due to different core systems is also reported.

© 2013 Elsevier B.V. All rights reserved.

## 1. Introduction

An enormous type of liquid crystals has been disclosed in the past wherein a wide variety of physical properties ranging from the dielectric, electro-optical, thermal conductivity to ferroelectric, fast switching ability and selectivity in reflecting light has been

associated with the versatility and workability of liquid crystals [1–4]. Among these liquid crystals, the supramolecular assemblies composed of oligomeric liquid crystals (LCs) and the liquid crystal compounds with obtuse and acute angled configurations have contributed tremendously toward the design of new liquid crystalline-based devices [5–7].

Recently the LCs particularly the liquid crystal dimers have received overwhelming attention owing to their ability to exhibit different phases and functionality as useful models for the semi-

\* Corresponding author. Fax: +60 4 6574854.

E-mail address: [gyeap@usm.my](mailto:gyeap@usm.my) (G.-Y. Yeap).

flexible and/or main-chain liquid crystal polymers such as liquid crystal oligomers containing semi-rigid mesogenic units connected via flexible spacers [8–14]. The salient feature of liquid crystal oligomers can be exemplified by the pronounced odd–even effect when the length of the spacer was varied [15,16].

In 1907, Vorländer has proposed a rule stating that ‘the liquid crystalline state is obtained for the most linear molecules’, but details of their molecular structure and micro-segregation have later attracted much attention for producing novel and self-assemblies compounds [17]. Later in 1929, Vorländer has reported the liquid crystalline properties of some compounds such as bis[4-(4-methoxy-phenylazo)phenyl]isophthalate and 1,2-phenylene bis-[4-(4-ethoxyphenylazo)benzoate] of which the molecules were presumed to possess obtuse and acute angled configurations, respectively [18–20]. Subsequently, Goring et al. had described tuning-fork-shaped molecules that showed undulated smectic structures [21] and Attard et al. reported Y-shaped molecules wherein three mesogenic groups were symmetrically connected to a phenyl ring [22]. Besides, the U-shaped LCs had also been investigated by several research groups [23–26]. Attard and Douglass had studied the structure-properties correlation of dimeric compounds derived from phthalic acid which had provided important insight on U-shaped LC systems [21]. The attempt by Jackson et al. to investigate the cyanobiphenyl-based LC dimers containing catechol as a linking group had also disclosed the odd–even effect as resulted from varying the parity of the spacer wherein the even derivatives possessed higher melting and clearing points [25,27].

Todate, the majority of work on bent, banana, – V- and U-shaped liquid crystals have been reported [28,29]. These types of molecular topology and their abilities to form mesophases have geared towards the investigation of molecular assembly as these molecular architectures are found to be important in

critical applications within a wide temperature range of functionality [4].

In view of this, we are prompted to employ catechol, 4,5-dibromocatechol, resorcinol, hydroquinone and 4,4'-dihydroxybiphenyl as core systems attached by the benzothiazole units. The thermal and optical behavior were investigated extensively with the aim of tapping the unique mesomorphic behavior among this series.

## 2. Experimental details

### 2.1. Materials

2-Amino-6-ethoxybenzothiazole and 1,10-dibromodecane were purchased from Acros Organics (New Jersey, USA). Whist sodium nitrite and phenol were obtained from M&R and Sigma, the catechol, resorcinol, hydroquinone and 4,4'-dihydroxybiphenylene were purchased from Aldrich. All solvents and reagents were used without further purification. 4,5-dibromocatechol was synthesized according to the reported method [30]. The synthetic route to prepare all the intermediates and target compounds with atomic numbering scheme are shown in Scheme 1.

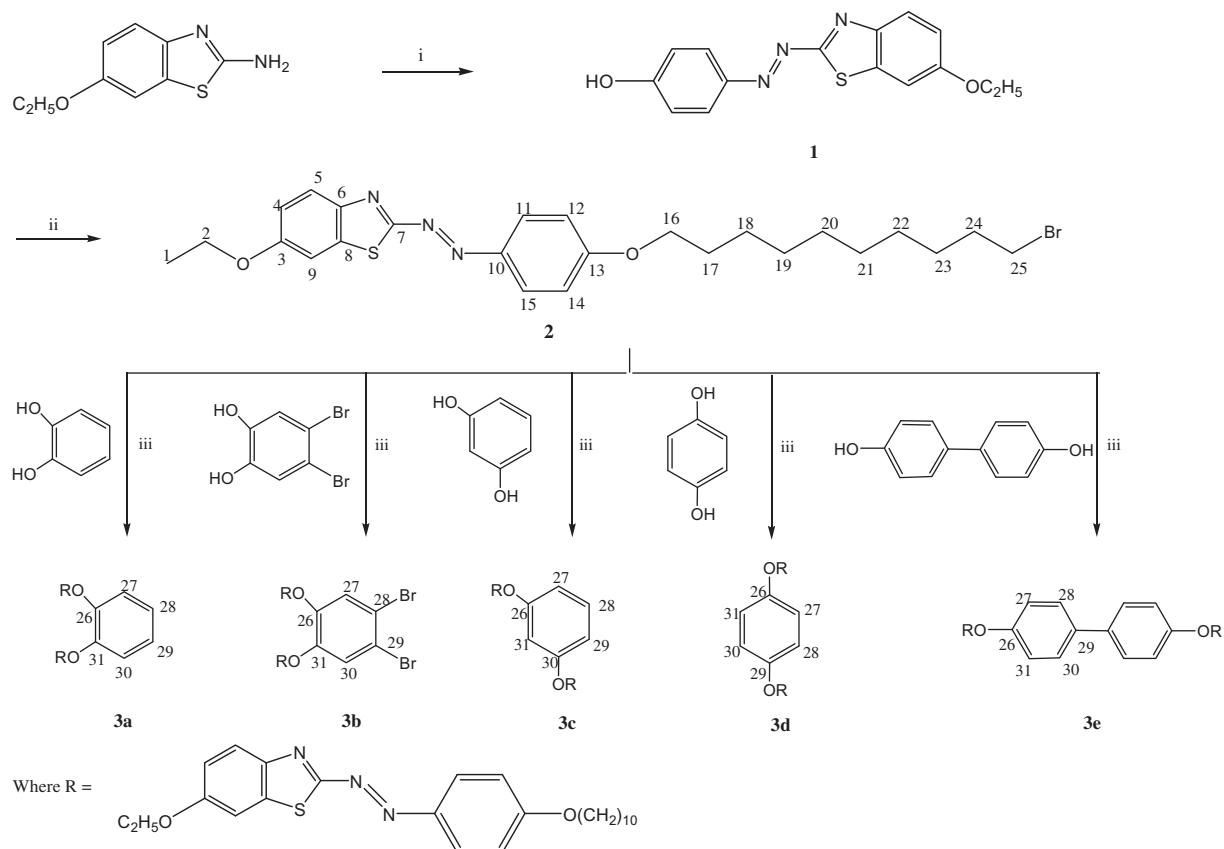
### 2.2. Characterization

#### 2.2.1. Physical measurements

Melting points were recorded by Gallenkamp digital melting point apparatus. The CHN microanalyses were carried out on Perkin–Elmer 2400 LS Series CHNS/O analyzer.

#### 2.2.2. FTIR measurement

Infrared spectra for all intermediates and title compounds were obtained from Perkin–Elmer 2000 FT-IR spectrophotometer in



**Scheme 1.** Synthetic route for the target compounds **3a–3e**. Reagent: (i)  $\text{NaNO}_2$ ,  $\text{H}_2\text{SO}_4$ , Phenol,  $\text{NaOH}$ ; (ii)  $\text{Br}(\text{CH}_2)_{10}\text{Br}$ ,  $\text{K}_2\text{CO}_3$ ,  $\text{KI}$ , Acetone; (iii)  $\text{K}_2\text{CO}_3$ ,  $\text{KI}$ ,  $\text{DMF}$ .

**Table 1**  
Phase transition temperatures and enthalpy changes for **3a–3e**.

Compound	Phase transition temperature, °C heating cooling (associated enthalpy change, kJ mol <sup>-1</sup> )
<b>3a</b>	Cr 69.0 (11.6) Cr <sub>1</sub> 75.8 (1.9) SmA123.0 (2.1) N 152.7 (1.0) I I 151.5 (1.4) N 122.1 (1.9) SmA <sup>a</sup>
<b>3b</b>	Cr 108.4 (15.1) SmA135.4 (1.6) N 145.4 (0.3) I I 144.9 (0.5) N 134.5 (1.9) SmA <sup>a</sup>
<b>3c</b>	Cr 122.7 (55.4) N 151.6 (2.0) I I 151.1 (2.1) N 125.4 (59.5) Cr
<b>3d</b>	Cr 189.0 (116.1) I I 183.1 (7.5) N 176.4 (79.3) Cr
<b>3e</b>	Cr 179.8 (29.6) N 226.0 (3.6) I I 221.1 (4.5) N 167.6 (31.2) Cr

Cr, crystal; N, nematic; I, isotropic.

<sup>a</sup> The formation of SmA was observed until room temperature.

which the samples were mixed with KBr in the range of 4000–400 cm<sup>-1</sup>.

### 2.2.3. NMR measurement

The <sup>1</sup>H- and <sup>13</sup>C NMR spectra were obtained using Bruker Avance 500 and ultrashield spectrometers equipped with ultrashield magnets. Standard Bruker pulse programs were used throughout the entire experiment [31]. The <sup>1</sup>H- and <sup>13</sup>C NMR data for target compounds were further substantiated with the aids of 2D <sup>1</sup>H–<sup>1</sup>H correlation spectroscopy (COSY), <sup>1</sup>H–<sup>13</sup>C heteronuclear multiple quantum correlation (HMQC) and <sup>1</sup>H–<sup>13</sup>C heteronuclear multiple bond correlation (HMBC) by using deuterated chloroform (CDCl<sub>3</sub>), dimethylsulphoxide (DMSO-*d*<sub>6</sub>) as solvents and tetramethylsilane (TMS) as internal standard.

### 2.2.4. Phase transition temperature and enthalpy values

The phase-transition temperature and associated enthalpy values were determined by using a differential scanning calorimeter Seiko DSC6200R operated at a scanning rate of ±5 °C min<sup>-1</sup> both on heating and cooling cycles.

### 2.2.5. Texture observation

Texture observation of the mesophase was carried out by using Carl Zeiss Axioskop 40 polarizing microscope equipped with a Linkam LTS350 hot stage and TMS94 temperature controller. The samples studied by optical microscope were prepared in thin film sandwiched between glass slide and cover.

### 2.2.6. X-ray diffraction study

The X-ray diffraction measurement on **3a** was carried out using a Bruker D8 Discover and GADDS system. The homeotropic alignment of the samples was obtained by slow cooling of a drop of the isotropic liquid below the clearing temperature. The X-ray beam was directed almost parallel to the substrate surface and

the temperature of the sample was controlled by an accuracy of 0.1°.

## 2.3. Synthesis

### 2.3.1. 4-((5-Ethoxybenzothiazol-2-yl)diazanyl)phenol (**1**)

This compound was obtained from our earlier reported method [32].

### 2.3.2. Synthesis of 4-((6-ethoxybenzothiazol-2-yl)diazanyl)bromodecanoxyphenyl (**2**)

A solution consisting of compound **1** (8.33 mmol) in 150 ml of dry acetone, potassium carbonate (62 mmol), a catalytic amount of potassium iodide (100 mg) and a fivefold excess of 1,10-dibromodecane (41.6 mmol) was refluxed for 24 h. K<sub>2</sub>CO<sub>3</sub> was removed from hot solution by filtration and the acetone was removed under reduced pressure. The product was recrystallized three times from ethanol whereupon the pure compound was isolated.

### 2.3.3. Synthesis of **3a–3e**

A mixture of compound **2** (100 mmol) and the desired dihydroxyl compounds (i.e. catechol, resorcinol, hydroquinone, 4,4'-dihydroxybiphenyl) (220 mmol) were dissolved in 30 ml dry DMF in the presence of K<sub>2</sub>CO<sub>3</sub> (500 mmol) and catalytic amount of KI (100 mg). The mixture was heated on the oil bath at 80 °C with continuous stirring for 48 h for **3a**, **3b** and **3c** whilst 24 h for **3d** and **3e**. The resulting solution was then cooled and poured in ice water to remove the inorganic materials and the precipitate thus formed was filtered and washed several times by water. The product was purified by column chromatography using CHCl<sub>3</sub> as eluent and finally recrystallized from DMF to yield the pure desired compounds.

## 3. Results and discussion

The analytical data for intermediate **2** and final compounds **3a–3e** are shown in Table 1. The yields are found to be more than 65% while the purity for each compound is also in agreement with respective empirical formula.

### 3.1. Anisotropic behavior

The phase sequences and related transition temperatures upon heating and cooling for **3a–3e** are listed in Table 1. All the textures observed under the polarized light have been identified through comparison with those reported in the literatures [33,34].

The texture observation reveals that the compounds **3a** and **3b** are enantiotropic N and SmA phase. Upon cooling **3a** from isotropic liquid, the nematic droplets appear and coalesce to form the classical schlieren texture with two-brush and four-brush defects (Fig. 1a). Further cooling has led to the appearance of fan shaped texture indicating the SmA phase which remains unchanged until

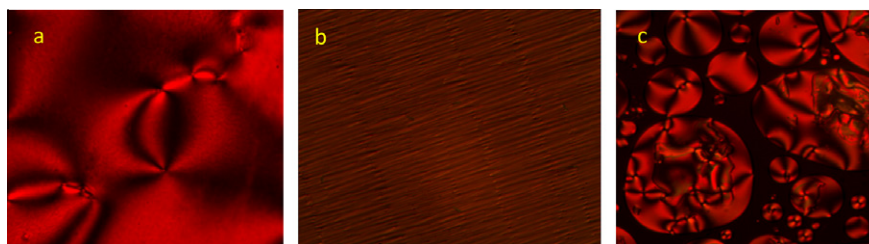


**Fig. 1.** Photomicrographs showing the (a) classical schlieren texture with two-brush and four-brush defects, (b) SmA texture for compound **3a**, (c) nematic schlieren texture for compound **3e**.

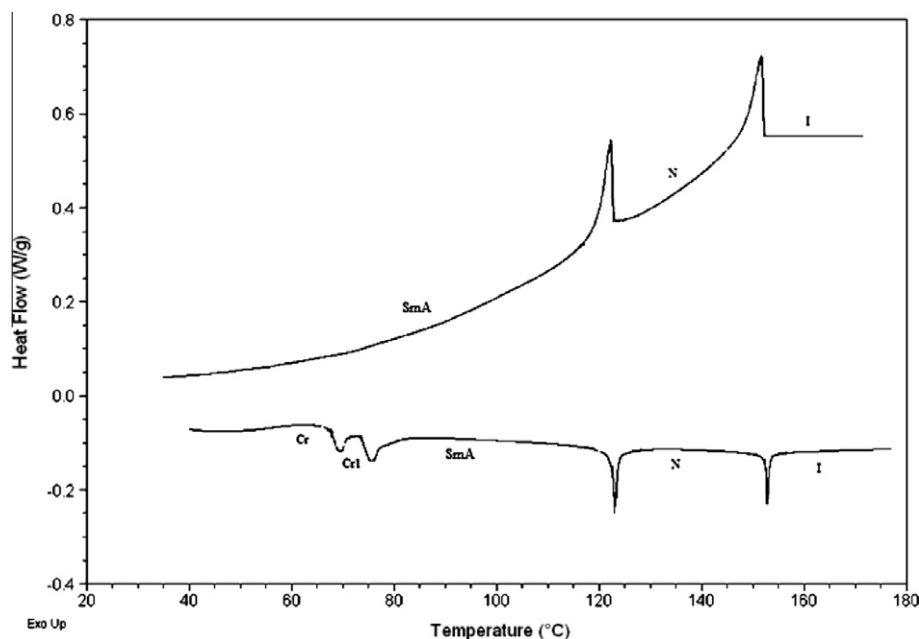


Fig. 2. DSC thermogram of compound **3a** upon heating and cooling.

room temperature (Fig. 1b). However, compounds **3c** and **3e** show enantiotropic N phase while compound **3d** is a monotropic nematic (Fig. 1c).

From the DSC thermogram for **3a**, there are two endotherms observable at 69.0 °C and 75.8 °C with enthalpies  $\Delta H = 11.6 \text{ kJ mol}^{-1}$  and  $1.9 \text{ kJ mol}^{-1}$  during the heating run and these can be assigned to Cr–Cr<sub>1</sub> and Cr<sub>1</sub>–SmA transitions, respectively. Subsequently, the third transition at 123.0 °C corresponds to SmA–N with  $\Delta H = 2.1 \text{ kJ mol}^{-1}$  followed by the transition of N–I at 152.7 °C in which the  $\Delta H = 1.0 \text{ kJ mol}^{-1}$ . However, upon cooling two peaks are observed at 151.5 °C and 122.1 °C with respective enthalpy values of  $1.4 \text{ kJ mol}^{-1}$  and  $1.9 \text{ kJ mol}^{-1}$  assignable to I–N and N–SmA transitions. There is no other peak which indicates the presence of SmA–Cr transition. Another interesting feature is that no sign of crystallization even the compound was left for 2 days at room temperature. However, a mechanical disturbance induces crystallization process (see Fig. 2).

### 3.2. Mesogenic properties and chemical constitution relationship

An extensive study upon the changes of mesomorphic properties resulted from the attachment of two identical mesogenic groups to different cores (i.e. catechol, 4,5-dibromocatechol, resorcinol, hydroquinone and dihydroxybiphenyl), wherein the alkyl spacer of C<sub>n</sub>H<sub>2n</sub> with  $n = 10$  remains intact, has been carried out.

Fig. 3 indicates that the phase transition temperatures are dependent on catechol, disubstituted catechol, resorcinol, hydroquinone and dihydroxybiphenyl. Whilst the present compounds **3a** and **3b** exhibit the phase sequence I–N–SmA–Cr, compounds **3c**, **3d** and **3e** are inclined to I–N–Cr. Moreover, by increasing the linearity there is a gradual increase in the clearing point from 152.1 °C (**3a**) to 226.5 °C (**3e**).

It can also be inferred from Fig. 3 that the thermal stability of SmA phase for compounds **3a** and **3b** are considered high wherein the temperature ranges upon heating are 97 °C and 109 °C, respectively. These values were obtained from the point where the compounds (**3a** and **3b**) show the SmA phase which persists until room temperature (25 °C). A comparison on the liquid crystalline proper-

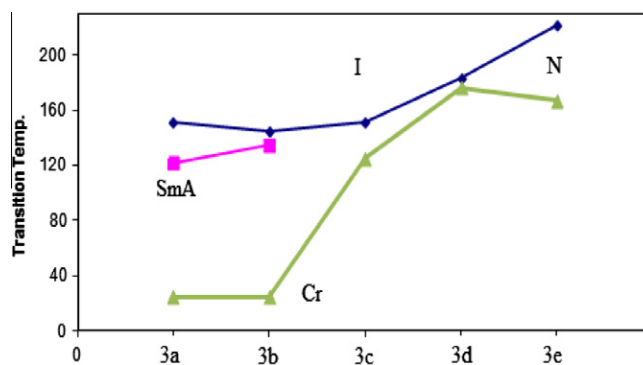


Fig. 3. The correlation between the transition temperatures and the target compounds possessing benzothiazole units at different positions.

ties between **3a** and **3b** reveals that both compounds **3a** and **3b** exhibit N and SmA phases. The thermal stability of SmA phase for **3a** is higher than **3b** by  $\Delta T_{\text{SmA}} = 20.2 \text{ °C}$  upon heating run. This phenomenon indicates that the bromine (Br) atoms are considered larger than the H atom and hence is more polarizable because the valence electrons are located far apart from the nucleus [35]. However, **3a** possesses higher nematic mesophase and thermal stability ( $\Delta T_{\text{N}} = 29 \text{ °C}$  and  $\Delta T = 126 \text{ °C}$ ) in comparison to **3b** ( $\Delta T_{\text{N}} = 10 \text{ °C}$  and  $\Delta T = 119 \text{ °C}$ ). This observation indicates that the lateral bromine substituent in **3b** has not only increased the breadth of the molecule but also the distorted planarity in the system due to steric interaction. These factors would decrease the nematic mesophase range and thermal stability for **3b** as compared with **3a** [36].

The linking position between mesogenic group and spacer varies from the *ortho* in **3a** to *meta* in **3c** until *para* in **3d**. Due to this molecular configuration characteristic, the compound **3a** is found to be more effective in enhancing the formation of the enantiotropic N and SmA phases. However, **3c** was found to exhibit enantiotropic N phase and compound **3d** shows monotropic N phase only. Furthermore, there is a clear crystallization except for **3a** and **3b**. Compounds **3a** and **3b** were found to show the phase sequence

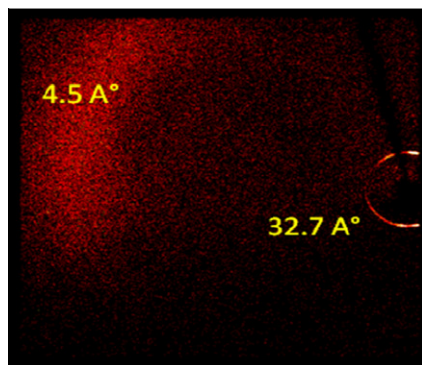


Fig. 4. XRD pattern for compound **3a**.

of I–N–SmA and compound (4,4' benzene derivative) **3e** shows the highest  $T_{I-N}$  transition.

The difference in the molecular geometry between compounds **3d** and **3e** lies in the number of phenyl rings. The presence of an additional phenyl ring in compound **3e** increases the molecular length and the overall polarizability of the molecule leading to stronger cohesive force at centre. Hence, it increases the aspect ratio for this compound and this can be exemplified by the greater nematic phase length and higher thermal stability of **3e** in comparison to compounds **3a**, **3b** and **3c** [37].

### 3.3. XRD study on compound 3a

In order to ascertain the nature of the smectic A phase formed by the symmetrical dimers, X-ray powder diffraction studies were carried out on **3a**. The X-ray pattern (Fig. 4) associated with the N and SmA phases for **3a** is shown in Fig. 4. The diffraction pattern shows a sharp reflection in the small angle region with  $d$  (molecular length) value of 32.7 Å corresponding to a typical signals for smectic phase with Bragg reflection. In the wide angle region a diffuse reflection is seen with a spacing of 4.5 Å corresponding to the intermolecular separation within the smectic layer due to the liquid-like positional correlation [38]. The calculated molecular length of the molecule **3a**, measured with Chem3D molecular model in which the calculated result derived from the MM2 is 32.5 Å (Fig. 5). Obviously the value 32.7 Å corresponds to the length of the molecule and the value  $d/l$  ratio is one. Thus, it is proven that the present dimer **3a** exhibits a monolayer SmA phase over a wide thermal range which includes the room temperature [39].

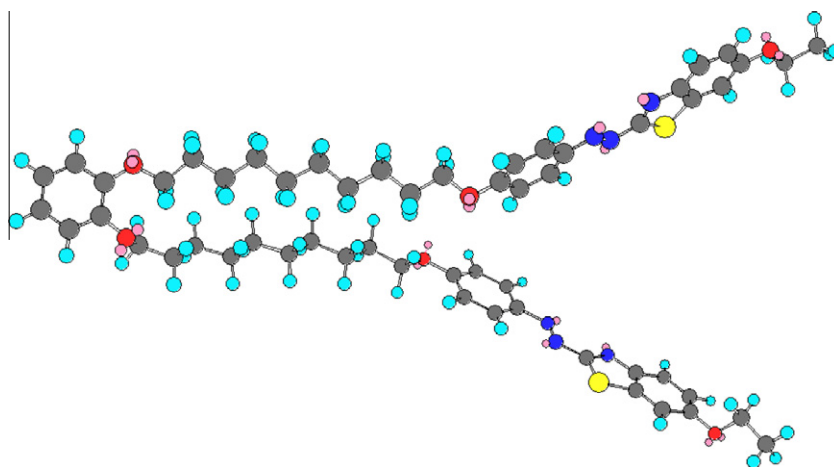


Fig. 5. The molecular shape of **3a** (energy-minimized model derived from CS ChemDraw Ultra 9.0).

### 3.4. Spectroscopic technique

From the FT-IR spectra (Table 2), a sharp peak at 2978–2852  $\text{cm}^{-1}$  indicates the presence of CH aliphatic bonds. The absorption band at 3069  $\text{cm}^{-1}$  is due to aromatic CH and the strong absorption band at 1598  $\text{cm}^{-1}$  corresponds to olefinic double bond (C=C). The absorption with a strong intensity at 1496–1470  $\text{cm}^{-1}$  can be assigned to aryl–alkyl ether linkage which substantiates the incorporation of the methylene spacer ( $\text{CH}_2$ ). The band at 1578  $\text{cm}^{-1}$  due to C=N from benzothiazol while the sharp peak at 1259  $\text{cm}^{-1}$  representing C–O stretching.

$^1\text{H}$  NMR spectral data of the compounds **3a–3e** are summarized in Table 3. The  $^1\text{H}$  NMR data show that the chemical shifts of **3a–3e** resonate as a triplet at  $\delta = 4.10$ –4.16 ppm and these can be assigned to methylene proton H2 whilst the resonances recorded within the range of  $\delta = 4.01$ –4.1 ppm and  $\delta = 3.92$ –3.99 ppm are attributed to methylene protons H16 and H25, respectively. The multiplet at  $\delta = 1.74$ –1.87 ppm corresponds to H17 and H24. The remaining methylene protons appear at  $\delta = 1.33$ –1.51 ppm with the triplet appears at  $\delta = 1.44$ –1.50 ppm can be assigned to the terminal methyl H1 proton. The aromatic protons for H11 and H15 were observed as doublet at  $\delta = 6.99$ –7.11 ppm and the protons for H12 and H14 which appear as doublet at  $\delta = 7.99$ –8.08 ppm. A singlet observed at  $\delta = 7.97$ –8.10 ppm can be attributed to aromatic proton H5. For the proton H9, it resonates as a singlet at  $\delta = 7.18$ –7.32 ppm. The H4 signal appears as doublet–doublet in the region of  $\delta = 7.01$ –7.13 ppm.

In **3a**, a remarkable upfield shift for the singlet at  $\delta = 6.88$  ppm represents H27–H30. However, in **3b**, the downfield shift of the singlet at  $\delta = 7.07$  ppm is assigned to protons H27 and H30.  $^1\text{H}$  NMR spectrum of **3c** exhibit a doublet at  $\delta = 6.45$  ppm, a singlet at  $\delta = 6.48$  ppm and a triplet at  $\delta = 7.14$  ppm which can be ascribed to protons H27, H29 with H31 and H28, respectively.

For **3d**,  $^1\text{H}$  NMR showed a singlet at  $\delta = 6.84$  ppm which can be assigned to protons H27–H31. For **3e**, the doublet at  $\delta = 6.95$  ppm and 7.44 ppm is caused by protons H28, H30 and H 27, H31, respectively.

$^1\text{H}$ – $^1\text{H}$  COSY results of compounds **3a–3e** are listed in Table 3. The correlation of the  $^1\text{H}$ – $^1\text{H}$  COSY experiment of compound **2** is employed to assign the aromatic and aliphatic protons (Table 3). Inspection from Fig. 6 for compound **2** suggests the correlation between H2 with the respective protons H1 and H3. A similar phenomenon can also be found on H4 which has correlated with H5. The correlation by COSY also reveals that the H11 and H15 protons from the aromatic ring are correlated with respective H12 and H14. The proton H4 or H5 is correlated with proton H6 or H7 and a sim-

**Table 2**  
Vibrational frequencies ( $\text{cm}^{-1}$ ) and their assignments for compounds **2** and **3a–3e**.

Compound	$\nu_{\text{C}_{\text{ph}}-\text{H}}$	$\nu_{\text{CH}_3}$	$\nu_{\text{CH}_2}$	$\nu_{\text{C}\equiv\text{C}}$	$\nu_{\text{C}\equiv\text{N}}$	$\delta_{\text{CH}}$	$\nu_{\text{C}-\text{O}}$
2	3077	2981	2851	1598	1578	1498–1971	1262
3a	3063	2978	2851	1598	1557	1498–1471	1256
3b	3070	2978	2852	1598	1578	1497–1471	1260
3c	3066	2977	2826	1598	1580	1497–1474	1254
3d	3069	2979	2852	1598	1576	1496–1472	1258
3e	3069	2978	2853	1598	1581	1498–1474	1246

$\nu$  = Stretching;  $\delta$  = bending.

**Table 3**  
 $^1\text{H}$  NMR chemical shifts ( $\delta/\text{ppm}$ ) of compounds **3a–3e**.

Atom no.	Chemical shift (ppm)				
	3a	3b	3c	3d	3e
H1	1.47	1.44	1.48	1.50	1.50
H2	4.12	4.10	4.13	4.16	4.16
H4	7.01	7.08	7.08	7.13	7.13
H5	8.01	7.99	8.01	8.04	8.10
H9	7.26	7.26	7.28	7.32	7.18
H11,15	7.07	6.99	7.02	7.11	7.10
H12,H14	7.99	7.97	7.99	8.02	8.08
H16	4.03	4.01	4.05	4.10	4.15
H17, H24	1.78, 1.82	1.76, 1.82	1.78, 1.82	1.77, 1.85	1.79, 1.87
H18–H23	1.34–1.49	1.32–1.45	1.33–1.48	1.36–1.51	1.38–1.51
H25	3.99	3.92	3.93	3.92	3.99
H27	6.88	7.06	6.48	6.84	7.45
H28	6.88	–	7.14	6.84	6.95
H29	6.88	–	6.48	–	–
H30	6.88	7.06	–	6.84	6.95
H31	–	–	6.45	6.84	7.45

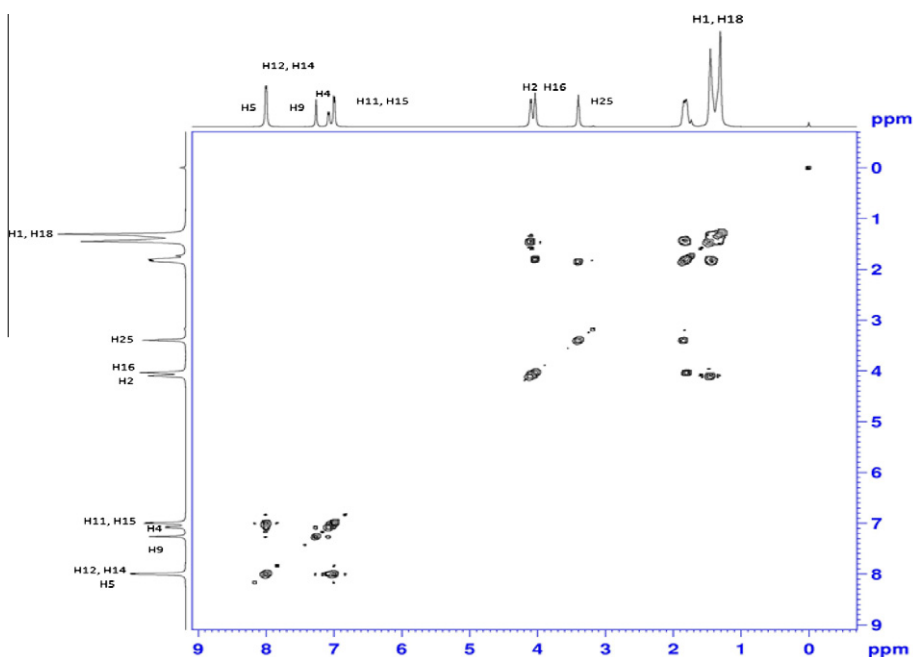
ilar phenomenon can also be found on H8 or H9 which has established connectivities with H10 or H11. Fig. 3 also shows that the ether group of proton H25 is correlated with the respective proton H24 and a similar phenomenon can also be found on H16 which has correlation with H17. The correlation inferred from COSY spectra has also shown that the H18, which has overlapped with proton

H1, can be correlated with H17. In the same way, a correlation can also be observed in compounds **3a–3e** with more correlations for aromatic protons attached to C25 in compound **2** by substitution reaction.

Table 4 summarizes the  $^{13}\text{C}$  NMR spectroscopic results of compounds **3a–3e**. The  $^{13}\text{C}$  NMR spectroscopy data for **3a** shows the peaks at  $\delta = 64.15$  ppm and 68.60 ppm which can be attributed to the C2 and C16. While a singlet at  $\delta = 69.30$  ppm represents the carbon C25 which has substantiated the formation of the ether bond with catechol. The C1 is observed at  $\delta = 14.78$  ppm whereas the remaining alkyl carbons are located at  $\delta = 25.29$ – $29.54$  ppm. The resonance due to aromatic carbons C4, C5, C9, C11 or C15 and C12 or C14 are observed at  $\delta = 116.52$  ppm, 125.44 ppm, 105.08 ppm, 115.08 ppm and 126.14 ppm, respectively. The resonances recorded at  $\delta = 114.26$  ppm and 121.07 ppm can be attributed to C28 or C29 and C27 or C30. On the other hand, the signals due to the quaternary aromatic carbons C3, C6, C7, C8, C10 and C13 are observed at  $\delta = 158.68$  ppm, 147.33 ppm, 173.94 ppm, 136.10 ppm, 146.12 ppm and 163.62 ppm, respectively. While the singlet at the low field ( $\delta = 149.29$  ppm) is due to C26 or C31.

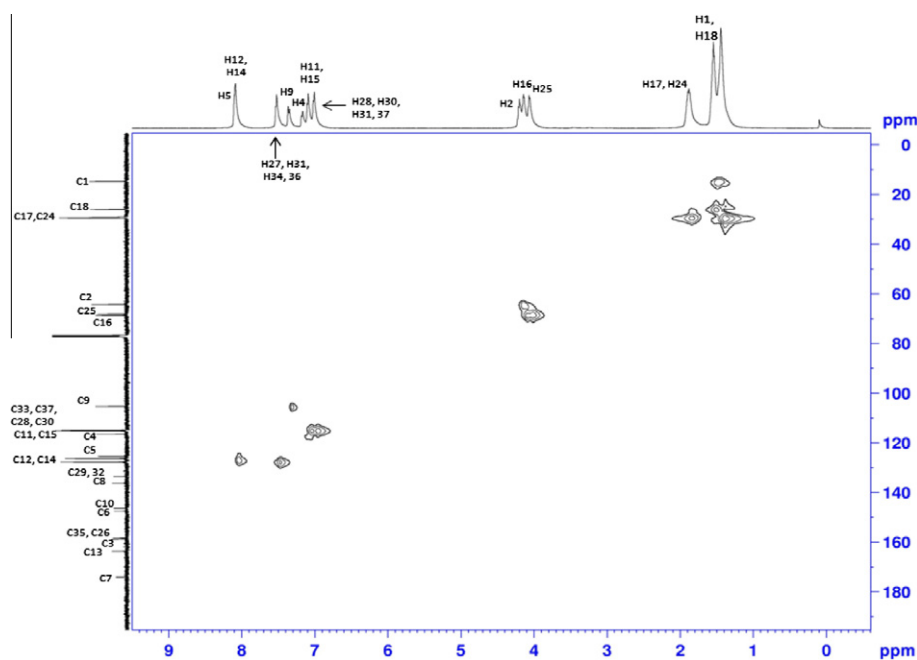
The  $^1\text{H}$ – $^{13}\text{C}$  HMQC spectra of compounds **2** and **3a–3e** provide the information on the interaction between the protons and the carbon atoms which are directly attached to each other (Tables 4 and 5, ESI†). As a representative, the discussion will be based on the spectrum of **3e** (Fig. 7). It can be deduced from Fig. 4 that the aromatic protons for H11 (magnetically equivalent to H15), H12 (magnetically equivalent to H14), H5, H4 and H9 in aromatic rings are correlated with C11 (magnetically equivalent to C15), C12 (magnetically equivalent to C14), C5, C4 and C9, respectively. A similar phenomenon can also be found on H27 (magnetically equivalent to H31, H34, H36) and H28 (magnetically equivalent to H30, H33, H37) in biphenyl ring which have correlated with C27 (magnetically equivalent to C31, C34, C36) and C28 (magnetically equivalent to C30, C33, C37), respectively. Moreover, the alkyl carbon atoms of C1, C2, C16, C17 or C24 and C25 show a cross peak with proton H1, H2, H16, H17 or H24 and H25, respectively.

The aromatic quaternary carbons for all compounds **2** and **3a–3e** were confirmed via the connectivities between the carbon and

**Fig. 6.**  $^1\text{H}$ – $^1\text{H}$  COSY spectrum of compound **2**.

**Table 4**  
<sup>13</sup>C NMR chemical shift for compounds **3a–3e**.

Carbon no.	Chemical shift (ppm)				
	<b>3a</b>	<b>3b</b>	<b>3c</b>	<b>3d</b>	<b>3e</b>
C1	14.78	14.78	14.79	14.77	14.79
C2	64.15	64.13	64.17	64.16	64.27
C3	158.68	158.67	158.70	158.69	158.81
C4	116.52	116.51	116.53	116.52	116.56
C5	125.44	125.42	125.46	125.43	125.52
C6	147.33	147.30	147.36	147.32	147.53
C7	173.94	173.91	173.96	173.95	174.04
C8	136.10	136.10	136.12	136.10	136.24
C9	105.08	105.05	105.12	105.11	105.36
C10	146.12	146.11	146.15	146.13	146.33
C11, C15	115.08	115.06	115.11	115.10	115.22
C12, C14	126.41	126.39	126.42	126.41	126.44
C13	163.62	163.59	163.65	163.65	163.74
C16	68.60	68.57	68.62	68.68	68.71
C17	29.54	29.49	29.47	29.45	29.48
C18, C23	25.99, 26.05	25.92, 25.98	25.97, 26.06	25.80, 25.95	26.01, 26.11
C19–C22	29.13–29.50	29.48–29.07	29.11–29.36	28.51–29.40	29.17–29.39
C24	29.54	29.49	29.47	29.45	29.48
C25	69.30	69.63	67.99	68.61	68.24
C26	149.29	149.09	160.41	153.24	158.39
C27	121.07	118.17	106.68	115.58	127.69
C28	114.26	114.74	129.76	115.58	114.95
C29	114.26	114.74	106.68	153.24	133.51
C30	121.07	118.17	160.41	115.58	114.95
C31	149.29	149.09	101.55	115.58	127.69
C32	–	–	–	–	133.51
C33, C37	–	–	–	–	114.95
C34, C36	–	–	–	–	114.95
C35	–	–	–	–	158.39

**Fig. 7.** <sup>1</sup>H–<sup>13</sup>C HMQC spectrum of compound **3e**.

its neighboring proton by HMBC correlation spectra. The aliphatic protons for all title compounds exhibit correlation with the attached aromatic ring carbon. However, the HMBC spectra of **3c** (Fig. 8) has shown that the H25, C16 and C2 are correlated with the carbons C26 or 30, and, C13 and C3 with <sup>2</sup>J. A similar phenomenon can also be found on H27 (magnetically equivalent to H29) which is correlated with C31 with <sup>2</sup>J. The quaternary carbons C10 and C13 are assigned based on correlations with H11 or H15 with

<sup>1</sup>J and <sup>2</sup>J, respectively. In addition, H12 or H14 is correlated with C13 and C10 with <sup>1</sup>J and <sup>2</sup>J, respectively. In the same way, H28 is also correlated with carbons C26 and C30 with <sup>2</sup>J. The H5 from the phenyl ring adjacent to nitrogen atom in thiazole ring is correlated with carbons C6 with <sup>1</sup>J, C8 and C3 with <sup>2</sup>J. In addition to the quaternary carbons, CH, CH<sub>2</sub>, CH<sub>3</sub> carbons are also used to establish the assignment with the aids of DEPT-90, DEPT-135 and DEPT-45 experiments.

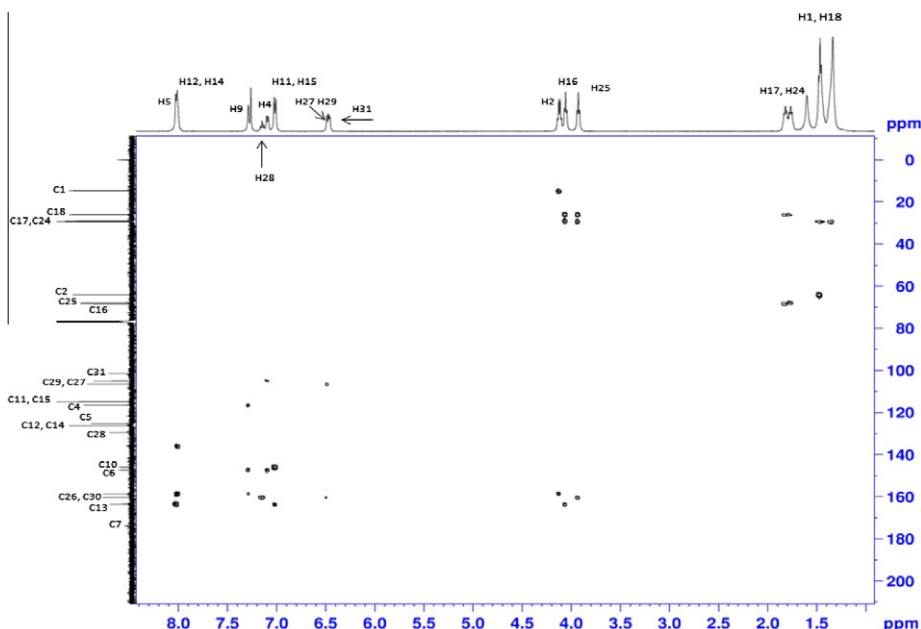


Fig. 8.  $^1\text{H}$ – $^{13}\text{C}$  HMBC spectrum of compound **3c**.

#### 4. Conclusion

A new series of dimeric compounds in which two mesogenic benzothiazole groups attached to different core units (catechol, 4,5-dibromocatechol, resorcinol, hydroquinone and 4-4'-dihydroxy-biphenyl) has been obtained through conventional method. Compounds with 1,2-substituted benzene (**3a**, **3b**) exhibit enantiotropic N and SmA phases. On the other hand, derivatives **3c** and **3e** show enantiotropic N phase while **3d** forms predominantly monotropic nematogen. The mesomorphic properties exhibited by the present series show that **3e** exhibits higher nematic phase stability as compared with other members in this series due to the increase in the breadth of the molecule.

#### Acknowledgments

The authors would like to thank Universiti Sains Malaysia for funding the project through FRGS Grant (Account No. 203/PKI-MIA/6711192). Authors also thank Ms Anna Zep and her supervisor Prof E. Gorecka for the powder X-ray diffraction measurement.

#### Appendix A. Supplementary material

Supplementary data associated with this article can be found, in the online version, at <http://dx.doi.org/10.1016/j.molstruc.2013.01.042>.

#### References

- [1] K. Kocevar, I. Muscivic, *Liq. Cryst. Today* 12 (2003) 3–8.
- [2] F. Simoni, L. Lucchetti, D.E. Lucchetta, O. Francescangeli, *Opt. Express* 9 (2001) 85–90.
- [3] L. Lucchetti, M.D. Fabrizio, O. Francescangeli, F. Simoni, *J. Nonlinear, Opt. Phys. Mater.* 11 (2002) 13–23.
- [4] R. Manohar, A.K. Misra, D.P. Singh, S.P. Yadav, P. Tripathi, A.K. Prajapati, M.C. Varia, *J. Phys. Chem. Solids* 71 (2010) 1684–1689.
- [5] (a) J.W. Goodby, G.H. Mehl, I.M. Saez, R.P. Tuffin, G. Mackenzie, R. Auzély-Velty, T. Benvegnu, D. Plusquellec, *Chem. Commun.* (1998) 2057; (b) I. Saez, J.W. Goodby, *J. Mater. Chem.* 15 (2005) 26–40.
- [6] C.T. Imrie, *Struct. Bond.* 95 (1999) 149–192.
- [7] R.W. Date, C.T. Imrie, G.R. Luckhurst, J.M. Seddon, *Liq. Cryst.* 12 (1992) 203–238.
- [8] C.T. Imrie, G.R. Luckhurst, in: D. Demus, J.W. Goodby, G.W. Gray, H.-W. Spiess, V. Vill (Eds.), *Handbook of Liquid Crystals*, vol. 2B, Wiley-VCH, Weinheim, 1998, pp. 801–833.
- [9] C.T. Imrie, P.A. Henderson, *Curr. Opin. Colloid Interface Sci.* 7 (2002) 298–311.
- [10] W. Weissflog, C.H. Lischka, S. Diele, I. Wirth, G. Pelzl, *Liq. Cryst.* 27 (2000) 43–50.
- [11] V. Prasad, K.H. Lee, Y.S. Park, J.W. Lee, D.K. Oh, D.Y. Han, et al., *Liq. Cryst.* 29 (2002) 1113–1119.
- [12] Y. Takamishi, T. Izumi, J. Watanabe, K. Ishikawa, H. Takezoe, A. Iida, *J. Mater. Chem.* 9 (1999) 2771–2774.
- [13] E.J. Choi, B.K. Choi, J.H. Kim, J.I. Jin, *Bull. Korean Chem. Soc.* 21 (2000) 110–117.
- [14] T. Ganicz, W.A. Stanczyk, E. Bialecka-Florjanczyk, I.Ś. Iedzińska, *Polymer* 40 (1999) 4733–4739.
- [15] P.A. Henderson, A.G. Cook, C.T. Imrie, *Liq. Cryst.* 31 (2004) 1427–1434.
- [16] P.A. Henderson, C.T. Imrie, *Liq. Cryst.* 32 (2005) 1531–1541.
- [17] D. Vorländer, *Chem. Ber.* 40 (1907) 1970–1972.
- [18] D. Vorländer, *Ber. Dtsch. Chem. Ges.* 63 (1929) 2831.
- [19] D. Vorländer, A. Apfel, *Ber. Dtsch. Chem. Ges.* 65 (1932) 1101–1109.
- [20] D. Vorländer, *Trans. Faraday Soc.* 29 (1933) 907–910.
- [21] P. Goring, G. Pelzl, S. Diele, P. Delavier, K. Siemensmeyer, K.H. Etzbach, *Liq. Cryst.* 19 (1995) 629–635.
- [22] G.S. Attard, A.G. Douglass, C.T. Imrie, *Liq. Cryst.* 11 (1992) 779–784.
- [23] H. Matsuzaki, Y. Matsunaga, *Liq. Cryst.* 14 (1993) 105–120.
- [24] G.S. Attard, A.G. Douglass, *Liq. Cryst.* 22 (1997) 349–358.
- [25] D. Jackson, M. Gossel, D. Ionescu, A. Johnston, G. Luckhurst, C. Schott, in: *Abstracts of 20th International Liquid Crystal Conference*, Ljubljana, Abstract No. SYN124, 2004.
- [26] T. Kato, H. Adachi, A. Fujishima, J.M.J. Frechet, *Chem. Lett.* 21 (1992) 265–268.
- [27] A. Yamaguchi, M. Watanbe, A. Yoshizawa, *Liq. Cryst.* 34 (2007) 633–639.
- [28] G.S. Attard, A.G. Douglass, C.T. Imrie, *Liq. Cryst.* 11 (1992) 779–789.
- [29] A. Yoshizawa, M. Nakata, A. Yamaguchi, *Liq. Cryst.* 33 (2006) 605–609.
- [30] M. Kohn, *J. Am. Chem. Soc.* 73 (1951) 480.
- [31] Bruker Program 1D WIN-NMR (Release 6.0) and 2D WIN-NMR (Release 6.1).
- [32] G.Y. Yeap, A. Alshargabi, M. Ito, W.A.K. Mahmood, D. Takeuchi, *Mol. Cryst. Liq. Cryst.* 557 (2012) 126–133.
- [33] D. Demus, L. Richter, *Texture of Liquid Crystals*, Verlag Chemie, New York, 1978.
- [34] I. Dierking, *Textures of Liquid Crystals*, Wiley-VCH, Weinheim, 2003.
- [35] T. Donaldson, H. Staesche, Z.B. Lu, P.A. Henderson, M.F. Archard, C.T. Imrie, *Liq. Cryst.* 37 (2010) 1097–1110.
- [36] G.W. Gray, *Steric Effects in Conjugated Systems*, Butterworth, London, 1958.
- [37] A.K. Prajapati, Vishal Modi, *Liq. Cryst.* 37 (2010) 407–415.
- [38] C.V. Yelamagad, I.S. Shashikala, U.D. Shankar Rao, S.K. Prasad, *Liq. Cryst.* 34 (2007) 153–167.
- [39] A. Marcelis, A. Kouidjs, E. Sudhölter, *Mol. Cryst. Liq. Cryst.* 411 (2004) 193–200.